Indian Journal of Geo Marine Sciences
Vol. 54 (08), August 2025, pp. 385-397
DOI: 10.56042/ijms.v54i08.12432

Research Article

A regional TSS retrieval model incorporating diffuse attenuation coefficient for a macro-tidal environment using satellite images: Gulf of Khambhat, India

S P Sakthivel[a], S Sundararajan[a], S K Dash[b] & B K Jena*[,a]

[a]Coastal Environmental Engineering Division, National Institute of Ocean Technology, Ministry of Earth Sciences, Government of India, Chennai, Tamil Nadu – 600 100, India

[b]National Centre for Coastal Research, Ministry of Earth Sciences, Government of India, Chennai, Tamil Nadu – 600 100, India

*[E-mail: bkjena.niot@gov.in]

Received 12 July 2024; revised 01 July 2025

A study of water quality parameters in the highly dynamic macrotidal region (ranging from 3 to 12 m) is required to reduce the high cost and labour intensity of field surveys. With advances in remote sensing technologies, it has become possible to utilise the enhanced spatial as well as temporal resolution of satellite image observations to estimate water quality parameters more accurately. This study proposes to develop a new regional model to estimate Total Suspended Sediment (TSS) by integrating Moderate Resolution Imaging Spectroradiometer (MODIS) images and field measurements for the dynamic region of the Gulf of Khambhat, India. This study uses regression analysis to develop and calibrate a new model using remote sensing reflectance and the diffuse light attenuation coefficient from MODIS images, along with field-measured TSS (obtained in December 2012 and March 2013). March 2015 data was used to validate the model. The regression coefficient (R2) of 0.8168, the root mean square error (RMSE) of 3.1 mg/L, and the mean relative error (MRE) of 0.3815 % are characteristics of the model, which will enable estimation of a wide range (60 mg/L to 2000 mg/L) of TSS values. The unique feature of the model is that results are obtained at 500 m resolution, using diffuse attenuation coefficient values calculated from MODIS images at 500 m instead of 1000 m resolution. With the availability of higher-resolution satellite images, the derived equation has been used to estimate TSS for recent years, particularly during the COVID-19 lockdown, when field data collection was not possible. Sentinel 2 MultiSpectral Instrument images have been used for the Gulf of Khambhat, and the derived TSS equation was applied to the study before, during, and after the COVID-19 lockdown.

[Keywords: COVID-19 lockdown, Diffuse attenuation coefficient, Macro tidal environment, Regression analysis, Remote sensing reflectance]

Introduction

Total Suspended Sediment (TSS) is a vital water-quality variable that provides information on the Gulf's highly dynamic seabed. Seabed sediments sourced from land erosion, biological, and microbial activities cover the tectonic features of the ocean floor. Suspended sediment in aquatic environments consists of three primary constituents: phytoplankton, detrital organic material, and inorganic mineral particles.. Routine in situ monitoring networks often have limited spatial and temporal coverage, making it difficult to obtain synoptic and regularly updated information on water quality. This led to a reliance on remotely sensed data for biogeochemical and hydrodynamic water-quality models to estimate the water-quality parameters. Numerous models have been derived from remotely sensed data (ocean colour imagery) from polar-orbiting satellites to estimate TSS parameter1-3. These models are primarily based on remote sensing reflectance measured at different wavelengths. Also, sensor characteristics, such as the temporal revisits and high spatial resolution, are important for accurately retrieving information needed to estimate the TSS.

The satellite based water-quality studies were carried out using Landsat images[4,5], SPOT Sea-viewing Wide Field-of-view Sensor (SeaWiFS)[5], Envisat MEdium Resolution Imaging Spectrometer (MERIS)[6], and IRS P4 Ocean Colour Monitor (OCM)[7]. Many studies have used MODerate resolution Imaging Spectroradiometer (MODIS) images for TSS parameter estimation, ranging from 250 m to 1000 m resolution[2,8-11]. Because of their global coverage of the dynamic coasts (twice a day) and spatial resolution (250 m to 1 km), MODIS imagery are often preferred for sediment studies.

Water quality exhibits considerable spatial variability among riverine, estuarine and coastal waters. Estimating TSS for the Gulf region is challenging due to its high dynamism, driven by tides

(3 to 12 m), ocean currents (1 m/s to 4 m/s), shallow shoals, and a movable seabed. The Gulf of Khambhat is a converging channel and experiences the highest tides of about 12 m on the Indian coast. It has diverse geomorphic features, including several estuaries, creeks, islands, mudflats, and salt marshes. Significant geomorphologic changes exist in the landforms and the shoreline of this region[12-14]. This indicates the dynamism of the Gulf. The field data collected from this region were used to develop the model. Thus, the model developed for such an area will indicate the robustness of the model. Hence, this study aims to create a new model for estimating TSS using MODIS images (Terra and Aqua) for the Gulf of Khambhat of India.

Knowledge of existing models for different locations is essential for developing a new model to estimate TSS. Many models have been developed using MODIS 250 m resolution images from other locations listed in Table 1. In most cases, one (645 nm) or two bands (645 nm, 855 nm) were used, and their reflectance values were correlated with *in-situ* TSS using various functions (linear, exponential, logarithmic, power, and polynomial functions).

The visible red channels are often used to map suspended sediments because they can discriminate the green pigment (Chlorophyll-*a*), highly turbid water, and TSS[refs. 2,21,22]. A single band at 250 m resolution showed better regression coefficient in closed or semi-enclosed lakes that show less complexity[2,9-11,15]. However, in dynamic and complex water bodies like bays and estuaries, the remote sensing reflectance of two bands at 250 m resolution has been used[8-10].

Wong *et al*.[16] used 500 m resolution MODIS images to estimate TSS in Hong Kong waters, which are turbid and influenced by Pacific currents and industrial effluents. The researchers also used 1000 m resolution images for TSS estimation, such as in Xian[17] and Wong *et al*.[16]. The use of 500 m and 1000 m resolution MODIS images indicates the contribution of the remote sensing reflectance of narrow bands at different wavelengths, rather than depending on the remote sensing reflectance of a single band or two bands at 250 m resolution. To estimate TSS concentrations, MODIS imagery at 250 m and 500 m spatial resolution were utilised.

The in-situ field data collection provides the basis for developing the TSS model. The in-situ sampling procedures comprised the selection of monitoring location, collection of water samples, transportation to the laboratory, TSS analysis and post-processing of the measured data. This approach represents the standard procedure for obtaining reliable TSS observation18. The estimation of TSS from field data involves either of the two standard methods: ASTM[ref. 19] or APHA[ref. 20]. Chen *et al*.[21] and Wang *et al*.[11] used the ASTM method of sample analysis, and Liquin[22] used the APHA method for suspended sediment analysis. The difference between the methods arises during sample preparation for subsequent filtering, drying, and weighing[23]. In the present study, APHA 21st Edition 2540 D has been used.

While existing studies highlight the use of spectral reflectance at multiple wavelengths for TSS estimation, most models rely on single- or dual-band relationships and provide limited representation of water-column optical processes[2,3]. This limitation becomes significant in highly dynamic environments such as the Gulf of Khambhat, where strong tidal forcing and high sediment loads influence light attenuation and sediment distribution[11,24]. Consequently, there is a need to incorporate physically meaningful indicator, such as the diffuse light attenuation coefficient (K_d), which better represent

Table 1 — The tidal range of the Gulf of Khambhat

West coast				East coast			
Location	Lat (N)	Long (E)	Tidal range (m)	Location	Lat (N)	Long (E)	Tidal range (m)
Veraval	20°54'	70°22'	2.6	Satpati	19°43'	72°42'	6.2
Diu Head	20°41'	70°50'	3	Tarapur	19°52'	72°40'	5.6
Nawabandar	20°45'	71°05'	2.8	Dahanu	19°58'	72°43'	5.6
Jafarabad	20°52'	71°23'	3.6	Umargam	20°12'	72°44'	6.8
Pipavav	20°57'	71°32'	3.6	Daman	20°25'	72°52'	7.6
Mahuva	21°03'	71°47'	6	Hazira	21°06'	72°37'	9
Gopnath	21°12'	72°07'	8	Kanthiajai	21°28'	72°40'	9.6
Alang	21°24'	72°12'	9.4	Luhara Point	21°39'	72°33'	10.2
Mithivirdi	21°29'	72°15'	10.6				
Bhavnagar	21°45'	72°15'	12.2				

subsurface optical variability[24]. Therefore, the present study integrates K_d with remote sensing reflectance to improve the robustness and accuracy of TSS estimation in optically complex coastal waters.

Materials and Methods

Study area

The Gulf of Khambhat (GoK) is prominent embayment of the Arabian Sea located along the state of Gujarat and lies between 20°00' N – 22°50' N latitude and 71°00' E – 73°00' E longitude (Fig. 1). It is 195 km wide at its mouth between Diu and Vadhavan and rapidly narrows to 24 km. The Gulf receives sediments from the Sabarmati, Mahi, Narmada, and Tapi rivers. It extends over an area of about 3120 square km, comprising predominantly characterised by extensive mudflats, interspersed with rocky shores and intertidal regions. In addition to these major rivers, several estuarine systems deliver a significant volumes of fresh water and sediment to the Gulf. Estuaries indent the coast around the Gulf of Khambhat and consist of extensive mudflats, dunes, and sporadic sandy beaches[25].

The Gulf is shallow at the periphery, while it is about 30 m deep in the middle. The coastal water is highly turbid, with very high concentrations of suspended sediments due to strong tidal mixing and resuspension of sediments[13]. The high turbidity of the Gulf (ranging from 1 to 6060 NTU) is due to high tidal inundation of the shallow regions and mudflats. Also, the rivers flowing through the area have a vast annual freshwater discharge of 38 km^3, carrying 74 million tons of sediments into the Gulf[25]. The imagery of the Gulf of Khambhat region is presented in Figure 1.

The samples were collected from various locations in GoK and subjected to laboratory analysis to determine suspended sediment concentration. Within the study area, 12 offshore and 10 river locations were selected to collect field data. The stations are chosen strategically to cover the entire Gulf region. These include 10 Peripheral River Stations (PRS) along the coast covering five rivers: Tapi (PRS1), Narmada

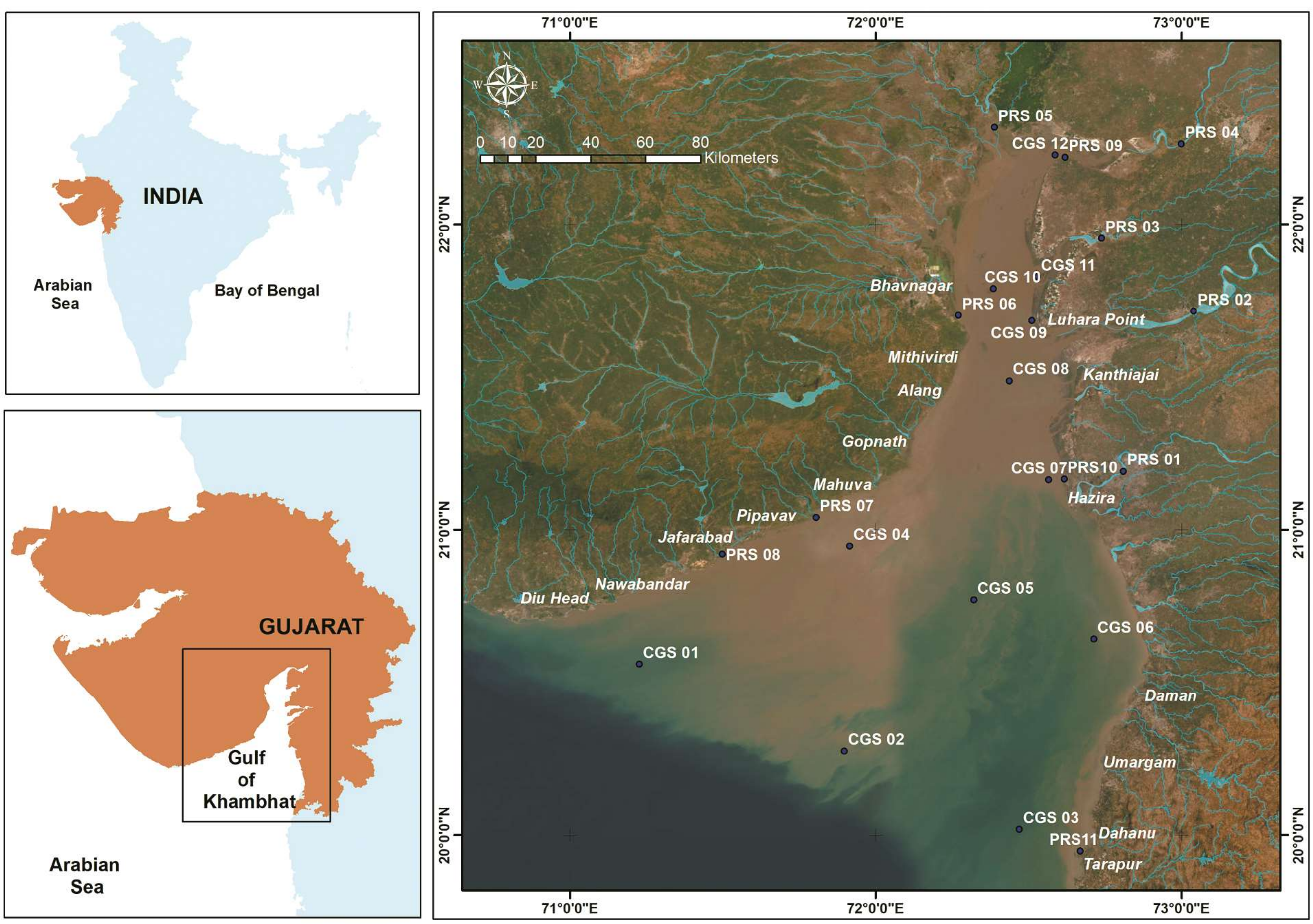

Fig. 1 — Location map showing the Gulf of Khambhat

(PRS2), Dhadhar (PRS3), Mahi (PRS4), and Sabarmati (PRS5) (Fig. 1). All the rivers are located on the eastern stretches of the Gulf, except the Sabarmati, which drains into the northern part of the Gulf. Three of the remaining five stations were located in the western Gulf (PRS 6, 7, 8) and the other two in the eastern Gulf (PRS 9, 10). Monthly sampling was performed in December 2012, March 2013, and March 2015, on spring and neap tide days (monthly) at low, mid, and high tide. 12 Central Gulf Stations (CGS) selected in the central Gulf, with six stations, are located on the southern side, while CGS 1 & CGS 4 are located on the western side of the Gulf, CGS 3 & CGS 6 are located in the eastern Gulf, and CGS 2 & CGS 5 are situated in the centre of the southern Gulf. Of the remaining six stations, CGS 7 is located near the mouth of the Tapi. CGS 8 & 9 are near the mouth of Narmada, CGS 10 & 11 are near the mouth of Dhadhar, and CGS 12 is located in the northern reaches of the Gulf.

GoK experiences a tidal range in excess of 12 m, which makes it second only to the Bay of Fundy of Canada in terms of large tidal ranges. The rapid amplification from 4 m at the mouth to 12 m within a 130 km distance into the Gulf may be attributed to the funnel shaped morphology of the Gulf. The tidal ranges of the Gulf of Khambhat on the east and west coasts are provided in Table 1.

***In-situ* TSS data**

Total suspended sediment represents the mass of suspended particulate matter per unit volume of water, determined gravimetrically as the fraction retained on atypically glass fibre filter with a nominal pore size of 0.7 µm and an effective pore size of 0.45 µm. The samples collected from the ten coastal stations and 12 offshore stations were analysed in the laboratory using the protocol prescribed by the APHA 21st Edition 2005[ref. 20]. As per the standard guidelines, a 1000 ml sample has to be collected and used, whereas, in this study, 500 ml of the samples was allowed to pass through the filter paper due to high turbidity and suspended sediment concentration. After careful removal from the filtration apparatus, the filter papers were dried for 1 hour at 103 – 105 °C. The filter papers were stored in desiccators to prevent moisture, and the final weight was measured. The difference between the final and initial weights gives the quantity of suspended solids per 500 ml of the sample, expressed as mg/L.

Satellite data

MODIS (Moderate Resolution Imaging Spectroradiometer) is multispectral earth observation sesnor developed by NASA aboard both Terra (Earth Observing System; EOS 10:30 AM) and Aqua (EOS 01:30 PM) satellites. The Terra satellite, launched in 1999crosses the equator on a north to south descending orbit at approximately 10:30 local time, whereas the Aqua, launched in 2004 follows a south to north ascending orbit around 13:30 local time. Together, these satellites provide near global coverage with frequent temporal observations of 1 to 2 days, acquiring spectral data in 36 bands (https://modis.gsfc.nasa.gov). These bands have spatial resolutions of 250 m, 500 m and 1 km, correspondng tobands 1 – 2, bands 3 – 7 and bands 8 – 36 respectively.

The effectiveness of MODIS bands 1 (620 – 670 nm) and 2 (841 – 876 nm) for mapping TSS concentrations under high turbidity conditions has been demonstrated in many studies[2,10,15]. In this study, cloud-free, atmospherically corrected level 2 data have been used at 250 m resolution MOD09GQ (MODIS Surface Reflectance Daily L2G Global 250 m) and 500 m resolution MOD09GA (MODIS Surface Reflectance Daily L2G Global 500 m) products for the dates and time synchronous with field data acquired and analysed (during December 2012, March 2013 and March 2015), as provided in Table 2. Despite the site's complexity, the field data were

Table 2 — Sensor specification of the satellite images used

Sensor	MODIS	Sentinel
Spatial resolution	250 m (bands 1 – 2) 500 m (bands 3 – 7) 1000 m (bands 8 – 36)	10 m (four visible and near-infrared bands), 20 m (six red edge and shortwave infrared bands), and 60 m (three atmospheric correction bands)
Swath width	2330 km (cross-track) by 10 km (along-track at nadir)	290 km
Spectral range	1 – 19 from 405 to 2155 nm 20 – 36 from 3.66 to 14.28 microns	443 – 2190 nm
No of bands	36	13
Quantisation	12 bits	12 bits
Date of acquisition	Daily TERRA and AQUA images of December 2012, March 2013, and March 2015	23rd January 2020; 27th April 2020; 3rd November 2020

collected synchronously with the satellite pass time. Such *in-situ* data has been used for regression analysis and validation.

In addition, Sentinel-2 MultiSpectral Instrument (MSI) sensor data were used to evaluate the applicability of the derived model at higher spatial resolution. Sentinel-2 provides 13 spectral bands ranging from visible to shortwave infrared with spatial resolutions of 10 m, 20 m, and 60 m. Level-2A products (Bottom-Of-Atmosphere surface reflectance) corresponding to January 2020 (pre-lockdown), April 2020 (during lockdown), and November 2020 (post-lockdown) were utilised. Sentinel-2 data have been increasingly applied to coastal water quality studies[26-28] due to their high spatial resolution and improved spectral capabilities.

The combined use of MODIS and Sentinel-2 datasets enables a multi-scale assessment, where MODIS provides high temporal resolution for capturing dynamic sediment variations, while Sentinel-2 offers high spatial resolution for detailed mapping of nearshore sediment distribution and estuarine processes.

Data pre-processing

Satellite data pre-processing is a critical step for ensuring accurate retrieval of water-leaving reflectance and reliable estimation of Total Suspended Sediments (TSS), particularly in optically complex and highly turbid coastal environments.

MODIS surface reflectance products (MOD09GQ and MOD09GA) were pre-processed using Quality Assurance (QA) filtering to remove cloud-contaminated and low-quality pixels, followed by subsetting to the study area. Surface reflectance was converted to Remote sensing reflectance (Rrs), and the diffuse light attenuation coefficient (K_d) was derived to account for water-column light attenuation, improving TSS estimation in highly turbid conditions[24,31].

Sentinel-2 MSI Level-2A data were further processed by applying cloud and shadow masking (using SCL), water masking, sun-glint correction, and band resampling to a common spatial resolution. The reflectance values were then converted to Rrs to ensure consistency with the modelling framework, which is essential for reliable TSS retrieval in optically complex waters[26,29,30]. Although Level-2A data are atmospherically corrected, uncertainties may persist in highly turbid waters; hence, specialised processors such as ACOLITE are often recommended for improved retrieval of water-leaving reflectance[26]. However, the applied corrections were found adequate for the present study.

Diffuse light attenuation coefficient (K_d)

The diffuse light attenuation coefficient, an indicator of water column turbidity, can be used for water quality applications where knowledge of light availability at different depths is needed. Suspended sediment in aquatic environment consists of primary constituents such as phytoplankton, detrital organic material, and inorganic mineral particles. Each of these components exhibits distinct optical characteristics that influence the interaction light with the water column. Phytoplankton absorbs light predominantly through their photosynthetic pigments, while other cellular material contributes lesser extent. In addition, phytoplankton scatters incoming light, primarily in the forward direction when their cells are relatively transparent. Certain algal species, such as coccoliths, possess highly reflective calcareous structures that enhance light scattering. Detrital organic matter generally has a brownish appearance, resulting in strong absorption within the blue and blue-green regions of the visible spectrum, while also contributing to light scattering. In contrast, mineral particles are typically light in colour and are characterised by their strong scattering properties, making them important determinant of water optical behaviour. A new model has incorporated a diffuse attenuation coefficient component, given the significance of the light propagation influenced by different components of suspended sediments. This will result in an improved model for estimating total suspended sediments in a region. Yang *et al.*[24] utilised the diffuse attenuation coefficient to predict chlorophyll and suspended sediments. The authors proposed using the diffuse attenuation coefficient to estimate suspended sediments in highly turbid waters.

K_d (490) mapped product is available at 1000 m resolution, but it has Not A Number (NaN) values for this study area. Hence, in the present study, the K_d values were reprocessed using the standard formula[31] for estimating K_d values from the Rrs 555 and Rrs 490 of the 500 m resolution MODIS image, as provided in Eq. 1.

$$K_d(490) = 0.016 + 0.1565\left[\frac{Lw\ (490)}{Lw\ (555)}\right]^{-1.540} \quad \ldots (1)$$

Remote sensing reflectance (Rrs) obtained from the MOD09GA product is defined as the ratio of water leaving radiance at wavelength λ to the down welling irradiance just beneath the sea surface (Eq. 2).

$$Lw(\lambda) = Rrs\ (\lambda) * E_d(\lambda) \quad \ldots (2)$$

Where, *Lw* (λ) is water-leaving radiance at wavelength λ, *Ed* (λ) is the down welling irradiance just beneath the sea surface, *Rrs* (λ) is remote sensing reflectance at wavelength λ, and $E_d(490)/E_d(555)$ is around 1.03 and varies slightly for different sun angles[24,32].

$$K_d(490) = 0.016 + 0.1565\left[1.03 * \frac{Rrs\ 490}{Rrs\ 555}\right]^{-1.540} \quad \ldots (3)$$

Since Rrs 490, available at 1000 m resolution, has the same issues as the K_d (490) mapped product, in this study, adopted Rrs 470, which is available at 500 m resolution in the blue region (provided in Eq. 4).

$$K_d(470) = 0.016 + 0.1565\left[1.03 * \frac{Rrs\ 470}{Rrs\ 555}\right]^{-1.540} \quad \ldots (4)$$

The values estimated from the above equation at 500 m resolution have been validated against the K_d values available at 1000 m resolution for the coverage area, except for the NaN values in the image. The model-calculated K_d values have been validated against available K_d values, with a correlation coefficient of 0.9442.

This study used the field-measured TSS values to develop and validate the model. For analysing and developing the model, 55 samples of MODIS 500 m and 250 m resolution images for 2012 and 2013 have been used. After eliminating the anomalous entities, 55 samples were reduced to 44 for MODIS 500 m resolution images and 36 for MODIS 250 m resolution images.

Model Study

TSS can be estimated empirically using the well-defined relationship between remote sensing reflectance in the green, red, or near-infrared spectral bands and the corresponding field-measured TSS concentration[2,8]. The present study considers the factors contributing to the estimation of TSS, as analysed by previous workers and studies conducted for the GoK region by Ankita *et al.*[33]. The overall workflow of the methodological framework for this study is shown in Figure 2. Satellite data processing,

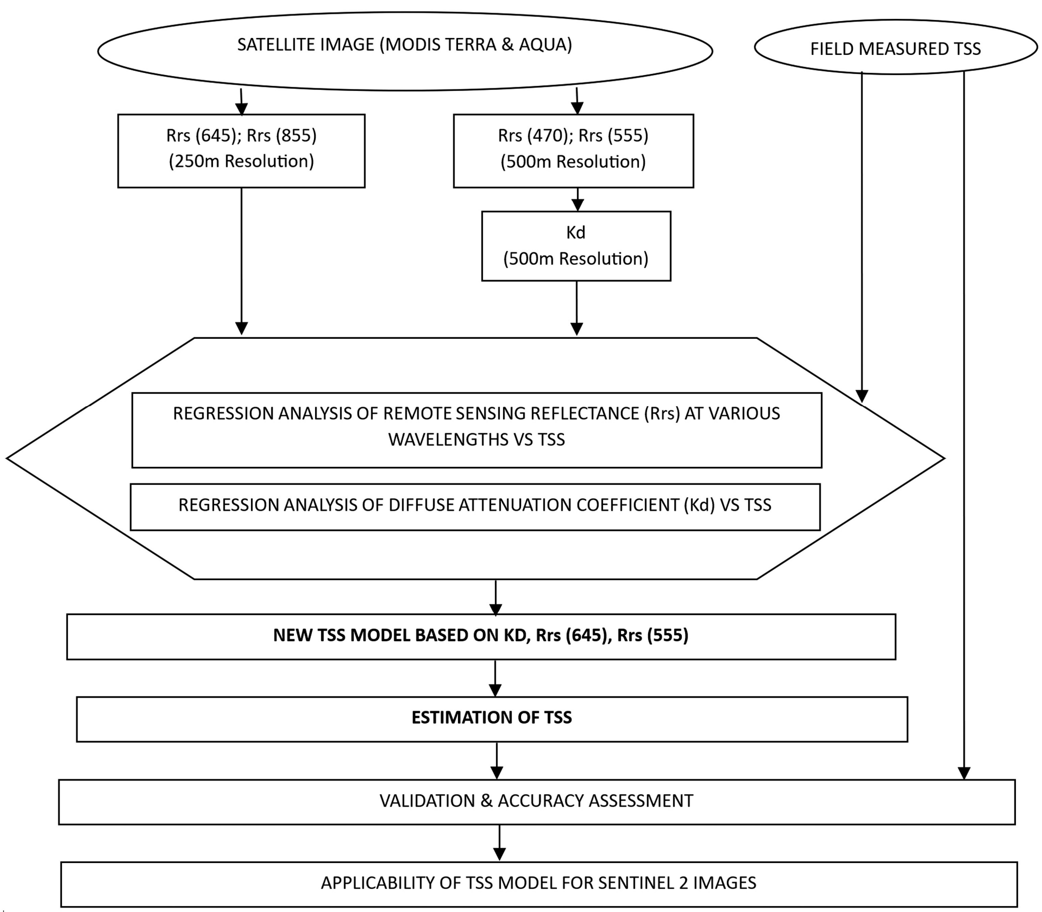

Fig. 2 — Flowchart depicting the methodology of the study

Table 3 — Linear correlation matrix of the seven bands with field-measured TSS

	645 nm	855 nm	470 nm	555 nm	1240 nm	1640 nm	2130 nm	K_d	TSS	log (TSS)
645 nm	1									
855 nm	0.5874	1								
470 nm	0.5059	-0.0271	1							
555 nm	0.7419	0.1278	0.9370	1						
1240 nm	0.2051	0.8090	-0.1567	-0.1123	1					
1640 nm	0.1238	0.4099	0.0730	0.0621	0.4647	1				
2130 nm	0.1746	0.7471	-0.1400	-0.1081	0.9743	0.4970	1			
K_d	0.0141	0.2897	-0.8207	-0.5966	0.2266	-0.0787	0.1929	1		
TSS	0.3235	0.2288	-0.2039	-0.0383	0.0452	-0.1587	-0.0021	0.5843	1	
log (TSS)	0.4708	0.3015	-0.0459	0.1234	0.0284	-0.0942	-0.0336	0.4509	0.9100	1

including data extraction and pre-processing, was carried out using SeaDAS and SNAP, while regression analysis and model development were performed in Microsoft Excel and MATLAB.

Results and Discussion

TSS measurement *vs.* existing models

Numerous models developed to estimate TSS from satellite images across locations have been evaluated. The low-to-moderate R^2 values do not indicate an appreciable correlation; hence, there is a need to develop a new model that incorporates factors such as regional dynamism driven by tides and winds. The models were based on the remote sensing reflectance from either a single spectral band or two spectral bands at 250 m resolution, whereas the correlation matrix (to be discussed in the following sections) indicates the dependency of other bands for the estimation of TSS at 500 m resolution.

TSS measurement *vs.* MODIS reflectance

The remote sensing reflectance of MODIS bands for 55 samples has been regressed against field-measured TSS values using regression analysis, as shown in Table 3. It can be seen that bands 1 (645 nm) and 2 (855 nm) show higher correlations of 0.471 and 0.307, respectively. Hence, the MODIS images of bands 1 and 2 at 250 m spatial resolution have been used to derive TSS.

The correlation matrix shows the response of the remote sensing reflectance in each spectral band to the variations in TSS values. TSS values depend on water clarity or turbidity, which can be estimated at the source. Further, K_d can be computed using equation (4).

The regression analysis between K_d and field-measured TSS values was carried out using 55 samples. The linear correlation matrix in Table 2 shows a higher correlation of K_d values with the field-measured TSS values (0.5843) than with 645 nm (0.3235). This indicates the need to include the K_d component in the new regional model to estimate TSS. K_d and TSS have been regressed using a second-order polynomial to further improve the correlation, yielding R^2 = 0.8324 (Fig. 3a). Since the *in-situ* TSS values are substantial, spanning from 120 mg/L to 1600 mg/L, the logarithmic function of TSS has been used for regression (R^2 = 0.6824; Fig. 3b). The spatial pattern of

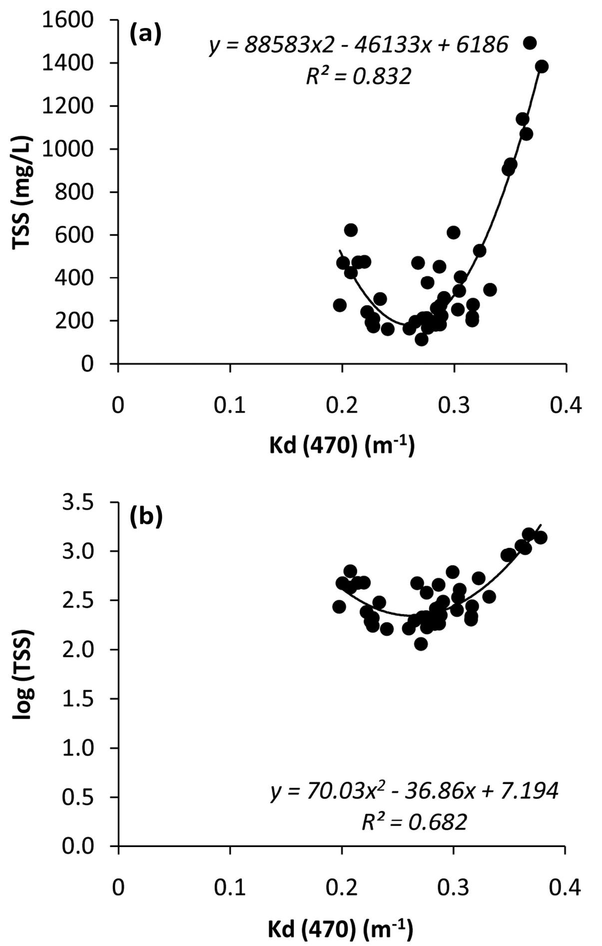

Fig. 3 — Regression analysis of diffuse attenuation coefficient (K_d) with field-measured TSS values and logarithmic function of TSS values

K_d values in the Gulf of Khambhat region is shown in Figure 4. Hence, the new regional model has been formulated based on the K_d and Band 1 of MODIS imagery at 500 m resolution.

Arnone *et al*.[34] used a combination of 1 km diffuse attenuation coefficient data with remote sensing reflectance from MODIS at 250 m resolution. Also, in a recent study by Xian[16], TSS was estimated using K_d values. It can be noted that previous studies used 1 km diffuse attenuation coefficient data, while in this study K_d values have been derived from 500 m resolution data.

The new model has been derived from the remote sensing reflectance of Rrs_{645} and Rrs_{855}, and the K_d component. The K_d values have been distributed in such a way that they match the logarithmic function of TSS field values, which formulate component '*K*' in the model Eq. 5. The difference of the remote sensing reflectance at 645nm and 855nm forms the X component in Eq. 6, used to develop the model. Components K and X of the model depict the contribution of the diffuse attenuation coefficient and remote sensing reflectance of bands 1 and 4. The final equation forrr deriving TSS values is provided in Eq. 7, where the model establishes a polynomial correlation with the logarithm of TSS.

$$K = 70.033{K_d}^2 - 36.863K_d + 7.1942 \quad \ldots (5)$$

$$X = (Rrs_{645} - Rrs_{855}) + K \quad \ldots (6)$$

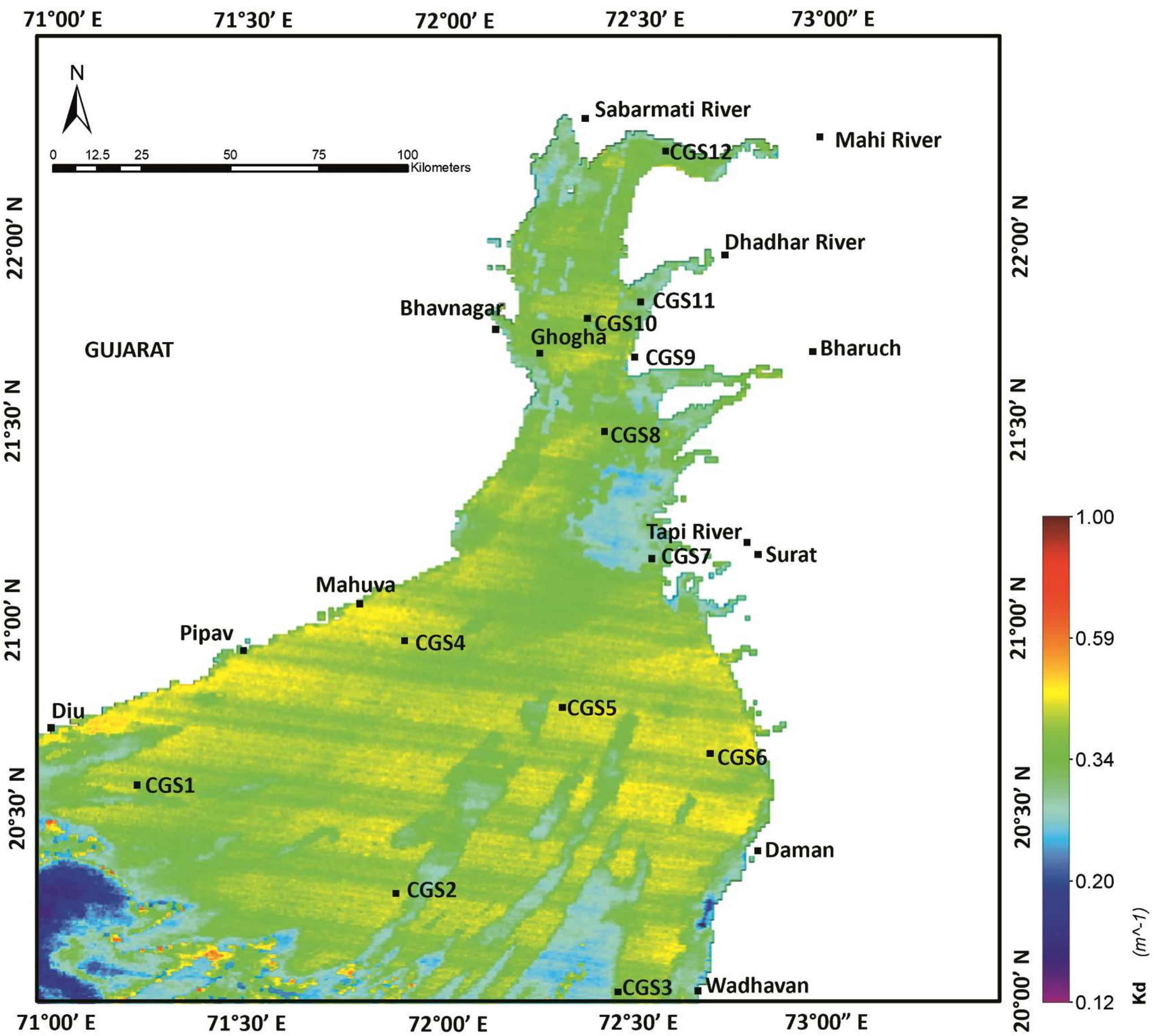

Fig. 4 — Map showing the distribution of diffuse attenuation coefficient (K_d) values for the GoK

$$\log TSS = 1.0572X^2 - 4.8425X + 7.9407 \quad \text{.... (7)}$$

The final equation has been derived based on 44 samples corresponding to the MODIS 500 m resolution images, which show a higher regression coefficient ($R^2 = 0.8$; Fig. 5), and the TSS levels range from 150 mg/L to1900 mg/L (Fig. 6).

The new model uses the relationship between TSS measurement and remote sensing reflectance of Band 1 (Rrs_{645}), Band 2 (Rrs_{855}), and Band 3 (Rrs_{470}), where the ratio of Band 3 and Band 4 has been used for the estimation of diffuse attenuation coefficient (K_d). A similar set of Rrs values at these wavelengths had been used for the analysis of TSS by Tassan[1], Pradhan *et al.*[35], and Pravin[7] for the Indian waters and the Gulf of Kutch region.

Model validation

The accuracy of the calibrated regional model using band 1 and the corresponding K_d derived from MODIS data to validate the model. Such validation of the models has been carried out earlier by several

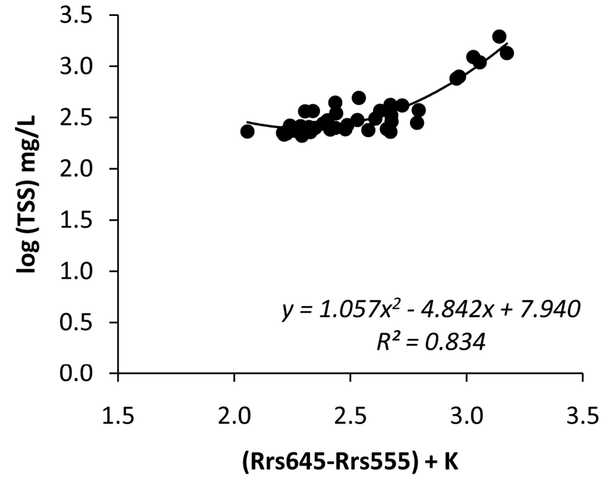

Fig. 5 — Graph showing the correlation coefficient between the new model and the logarithmic TSS values

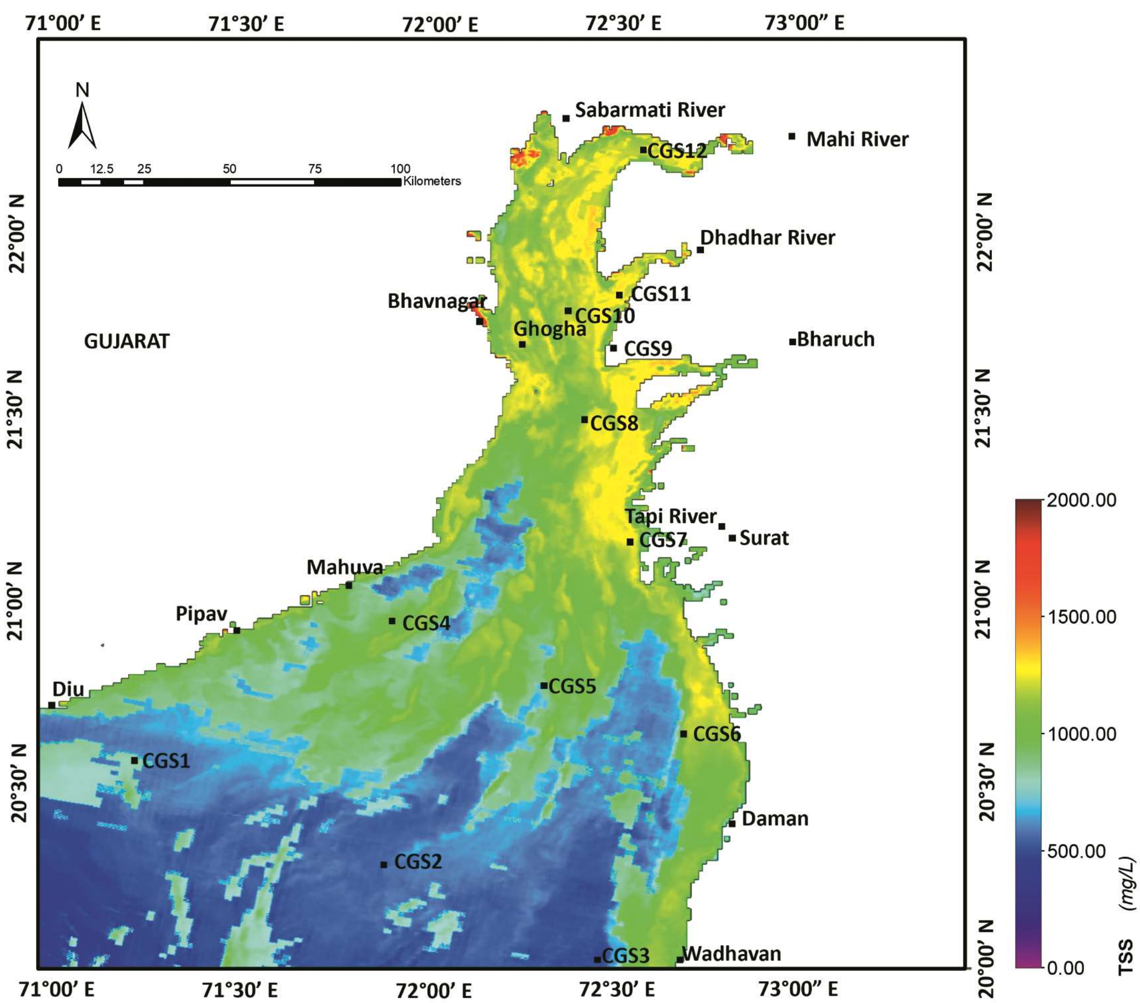

Fig. 6 — Map showing the distribution of Total Suspended Sediment (TSS) values for the GoK

researchers[6,21]. The present study estimates RMSE (Root Mean Square Error) and MRE (Mean Relative Error). The RMSE associated with TSS estimation is determined using Eq. 8.

$$\mathrm{RMSE} = \left[\sum \left(\mathrm{TSS}_{\mathrm{measured}} - \mathrm{TSS}_{\mathrm{predicted}}\right)^2 / \mathrm{N}\right]^{0.5} \quad \dots (8)$$

Where, $TSS_{measured}$ is TSS measured in the field, $TSS_{predicted}$ is TSS concentration estimated by the retrieval models, and N denotes the degree of freedom. The mean relative error associated with TSS estimation is computed using Eq. 9.

$$MRE = \left[100 \times \left|TSS_{measured} - TSS_{predicted}\right| / TSS_{measured}\right]\% \quad \dots (9)$$

The goodness of fit of each model can be assessed from the coefficient (R^2), RMSE, and MRE. Field samples ranging from 240 to 500 mg/L were employed to evaluate the model performance. However, the model has been designed to estimate TSS ranging from 60 to 2000 mg/L. The estimated regression coefficient and their corresponding metrics are displayed in Figure 7.

Case study during the COVID-19 pandemic

To examine the applicability of the developed TSS model, a case study was carried out using 10 m Sentinel-2 MultiSpectral Instrument (MSI) imagery. The model was applied to three temporal scenarios: pre-lockdown (January 2020), during lockdown (April 2020), and post-lockdown (November 2020), and the resulting TSS distributions are presented in Figure 8.

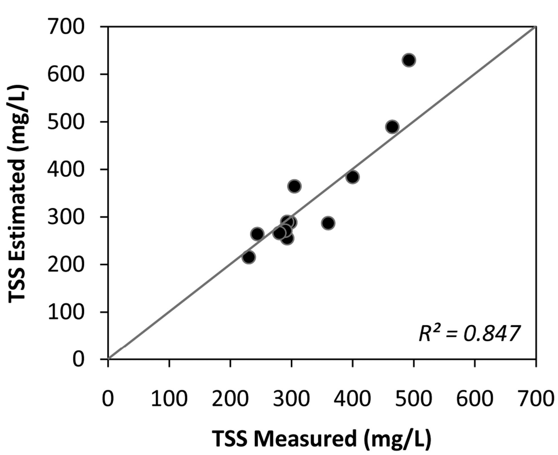

Fig. 7 — Validation of the new model showing the correlation coefficient and the errors between the new model and the logarithmic TSS values

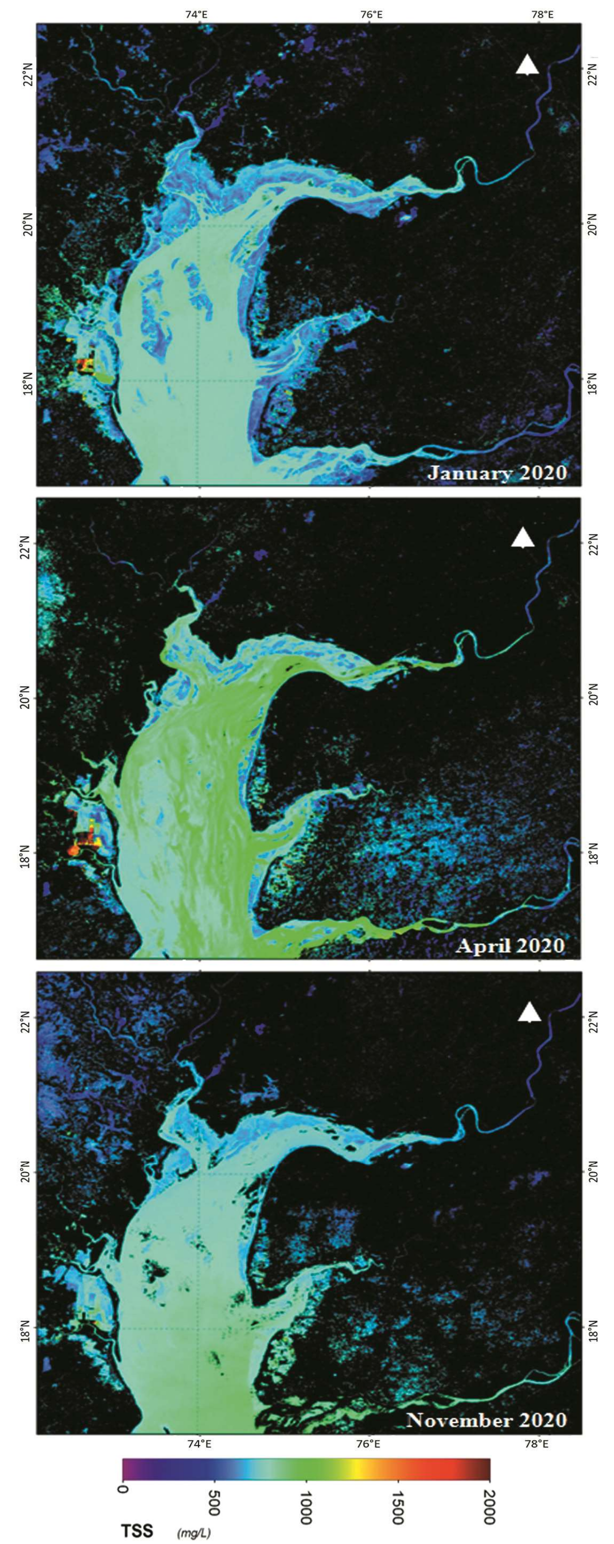

Fig. 8 — TSS estimation for the part of the Gulf of Khambhat for the dates before (January 2020), during (April 2020), and after (November 2020) the COVID-19 lockdown using the available Sentinel 2 MSI satellite images. Note: Black colour denotes land mask

The results indicate that suspended sediment concentrations were relatively higher in April 2020 compared to January and November 2020. This variation can primarily be attributed to seasonal influences, such as elevated temperatures and reduced freshwater discharge during summer, which enhance sediment resuspension and concentration in coastal waters[11,24]. The finer spatial resolution and diverse spectral bands in Sentinel-2 imagery enable improved delineation of nearshore sediment plumes and estuarine gradients, thereby enhancing the interpretation of localised sediment dynamics[26-28].

Field-based data collection in such a highly dynamic macrotidal environment is inherently challenging and was further constrained during the COVID-19 lockdown. In this context, satellite-based estimation of TSS using a region-specific calibrated model provides a reliable and efficient alternative for monitoring suspended sediment variability[3,29]. Furthermore, recent multi-sensor studies highlight the growing capability to integrate data from MODIS, Sentinel-2, and other platforms to facilitate the retrieval of water quality variables across spatial-temporal scales[26,29]. The results demonstrate that the developed model can effectively capture temporal variations in TSS and highlight its applicability for multi-sensor integration and operational coastal water quality assessment, particularly in data-scarce and highly dynamic environments.

Conclusion

This study presents a region-specific and improved empirical approach for retrieving Total Suspended Sediments (TSS) in a highly dynamic macro-tidal environment of the Gulf of Khambhat using MODIS imagery. The developed model demonstrates reliable performance over a broad range of TSS levels, particularly under highly turbid coastal and estuarine waters.

The key novelty of the study lies in integrating the diffuse light attenuation coefficient (K_d) with Rrs observations at 645 nm and 555 nm, providing a more physically representative framework for TSS estimation. The model shows strong predictive capability for TSS values exceeding 200 mg/L, with $R^2 = 0.8168$, RMSE = 3.1 mg/L, and MRE = 0.3815 %. Furthermore, deriving K_d at 500 m spatial resolution from MODIS reflectance enhances spatial consistency compared to conventional approaches that rely on coarser-resolution products.

Unlike conventional models that primarily rely on individual spectral bands, the present approach uses the ratio of remote sensing reflectance to estimate K_d, which is subsequently integrated into a polynomial regression framework based on logarithmic TSS values. This demonstrates that inclusion of physically meaningful optical parameters significantly improves model robustness and applicability in optically complex waters.

The model's applicability was further validated using Sentinel-2 MSI data, which enabled high-resolution mapping of sediment dynamics during pre-, during, and post-COVID-19 conditions. The results confirm that the developed model is transferable across sensors, supporting multi-scale analysis by combining the frequent revisit capability of MODIS with the finer spatial resolution of Sentinel-2[refs. 26-29].

With the increasing availability of multi-sensor satellite datasets, there is significant potential to advance coastal water quality monitoring. Beyond TSS estimation, the proposed methodology has potential for extension to other water quality indicators including chlorophyll-*a*, turbidity, and Coloured Dissolved Organic Matter (CDOM), whose concentration influence the optical characteristics of the water column[24,29,30]. The incorporation of parameters such as K_d and multi-band reflectance can improve the accuracy of retrieval for these variables, particularly in complex coastal environments.

The integration of advanced data-driven approaches, including machine learning and artificial neural networks, enables the development of more generalised and robust models. While empirical models offer simplicity and interpretability, AI/ML-based approaches can capture nonlinear relationships and complex interactions among spectral and environmental variables, thereby enhancing predictive performance in highly dynamic systems[3,11].

The findings demonstrate the feasibility of developing scalable, hybrid, and multi-sensor frameworks for effective monitoring of coastal water quality. Future work should focus on improving model generalisation, incorporating larger datasets, and developing globally applicable approaches to reduce dependence on extensive field measurements and enable efficient, operational monitoring of coastal environments.

Acknowledgements

The authors gratefully acknowledge the support and encouragement provided by the Director of the

National Institute of Ocean Technology (NIOT) in Chennai; Dr M. V. Ramana Murthy, Former Director of the National Centre for Coastal Research (NCCR); and Former Group Head of Coastal and Environmental Engineering, NIOT, Chennai..The authors also thank all project personnel who contributed to field data collection under the Ministry of Earth Sciences (MoES) funded Shoreline Management Project. In addition, a portion of the dataset used in this study was obtained through an externally sponsored research project.

Author Contributions

SPS: Analysis of satellite images and writing of the manuscript; SS: Measurements and data collection of water samples; SSD: Concept of analysis and formulation; and BKJ: Planning, execution and supervision of work.

References

1 Tassan S, Local algorithms using SeaWiFS data for the retrieval of phytoplankton, pigments, suspended sediment and yellow substance in coastal waters, *Appl Opt*, 33 (12) (1994) 2369-2378. https://doi.org/10.1364/AO.33.002369

2 Miller R L & McKee B A, Using MODIS Terra 250 m imagery to map concentrations of total suspended matter in coastal waters, *Remote Sens Environ*, 93 (1–2) (2004) 259–266. https://doi.org/10.1016/j.rse.2004.07.012

3 Chen S, Han C, Chen X, Li D, Sun L, *et al*., Estimating wide range Total Suspended Solids concentrations from MODIS 250m imageries: An improved method, *ISPRS J Photogramm Remote Sens*, 99 (2015) 58-69. https://doi.org/10.1016/j.isprsjprs.2014.10.006

4 Topliss B J, Almos C L & Hill P R, Algorithms for remote sensing of high concentration, inorganic suspended sediment, *Int J Remote Sens*, 11 (6) (1990) 947–966. http://dx.doi.org/10.1080/01431169008955069

5 Doxaran D, Froidefond J M & Castaing P, Remote-sensing reflectance of turbid sediment-dominated waters. Reduction of sediment type variations and changing illumination conditions effects by use of reflectance ratios, *Appl Opt*, 42 (15) (2003) 2623–2634. https://doi.org/10.1364/AO.42.002623

6 Xi H & Zhang Y, Total suspended matter observation in the Pearl River Estuary from in situ and MERIS data, *Environ Monit Assess*, 177 (1) (2011) 563-574. https://doi.org/10.1007/s10661-010-1657-3

7 Pravin K, Sediment concentration and bed form structures of Gulf of Cambay from remote sensing, *Int J Remote Sens*, 29 (8) (2008) 2169-2182. https://doi.org/10.1080/01431160701422221

8 Ondrusek M, Stengel E, Kinkade C S, Vogel R L, Keegstra P, *et al.*, The development of a new optical total suspended matter algorithm for the Chesapeake Bay, *Remote Sens Environ*, 119 (2012) 243-254. https://doi.org/10.1016/j.rse.2011.12.018

9 Chen S S, Huang W R & Chen X Z, An enhanced MODIS remote sensing model for detecting rainfall effects on sediment plume in the coastal waters of Apalachicoa Bay, *Mar Environ Res*, 72 (5) (2011) 265-272. https://doi.org/10.1016/j.marenvres.2011.09.014

10 Doxaran D, Froidefond J M, Castaing P & Babin M, Dynamics of the turbidity maximum zone in a macrotidal estuary (the Gironde, France): Observations from field and MODIS satellite data, *Estuar Coast Shelf Sci*, 81 (3) (2009) 321–332. http://dx.doi.org/10.1016/j.ecss.2008.11.013

11 Wang F, Zhou B, Xu J, Song L & Wang X, Application of neural network and MODIS 250 m imagery for estimating suspended sediment concentration in Hangzhou Bay, China, *Environ Geol*, 56 (6) (2008) 1093–1101. https://doi.org/10.1007/s00254-008-1209-0

12 Shaik M G, Nayak S, Shah P N & Jambusaria B B, Coastal landform mapping around the Gulf of Khambhat using Landsat TM data, *J Indian Soc Remote Sens*, 17 (1) (1989) 41-48. https://doi.org/10.1007/BF02995964

13 Gupta M, Monitoring Shoreline Changes in the Gulf of Khambhat, India During 1966-2004 Using RESOURCES AT-1 LISS-III, *Open J Remote Sens Pos*, 1 (1) (2014) 27-37. https://doi.org/10.15764/RSP.2014.01003

14 Misra A & Balaji R, A study on the shoreline changes and Land-use/land cover along the South Gujarat coastline, *Procedia Eng*, 116 (2015) 381-389. https://doi.org/10.1016/j.proeng.2015.08.311

15 Cui L, Qiu Y, Fei T, Liu Y & Wu G, Using remotely sensed suspended sediment concentration variation to improve management of Poyang Lake, China, *Lake Reserv Manag*, 29 (1) (2013) 47-60. https://doi.org/10.1080/10402381.2013.768733

16 Wong M S, Nichol J E, Lee K H & Emerson N, Modeling water quality using terra/modis 500 m satellite images, In: *The International Archives of the Photogrammetry, Remote Sensing and Spatial Information Sciences*, Vol XXXVII, Part B8, Beijing, 2008, pp. 679-684.

17 Xian G Z, *Remote sensing application for the urban environment*, 1st edn, Taylor & Francis Series in Remote sensing Applications, (CRC Press Inc, UK), 2015, pp. 220. ISBN 9781420089844

18 Edwards T K & Glysson G D, *Field methods for measurement of fluvial sediment*, US Geological Survey Open-File Report, 1988, pp. 86-531.

19 ASTM, *Standard Test Method for Determining Sediment Concentration in Water Samples*, American Society of Testing and Materials, D 3977-97 11.02, 1999, pp. 389-394.

20 APHA, *American Water Works Association, and Water Pollution and Control Federation, 1995, Standard Methods for the Examination of Water and Wastewater, (1995), Total Suspended Solids Dried at 103°-105° C, Method 2540D*, American Public Health Association, Washington DC, 1995, pp. 2-56.

21 Chen J, D'Sa E, Cui T & Zhang, A semi-analytical total suspended sediment retrieval model in turbid coastal waters: A case study in Changjiang River Estuary, *Opt Exp*, 21 (11) (2013) 13019-13031. https://doi.org/10.1364/OE.21.013018

22 Liqin Q, *Remote Sensing Suspended Sediment Concentration in the Yellow River*, Doctoral Dissertation, Submitted to University of Connecticut, 2014, pp. 383.

23 Gray J R, Glysson G D, Turcios L M & Schwarz G E, *Comparability of suspended-Sediment Concentration and Total Suspended Solids Data*, US Geological Survey Water-

Resources Investigations Report 00-4191, 2000, pp. 14. Accessed online at: http://water.usgs.gov/osw/pubs/WRIR00-4191.pdf

24 Yang C, Ye H & Tang S, Seasonal Variability of Diffuse Attenuation Coefficient in the Pearl River Estuary from Long-Term Remote Sensing Imagery, *Remote Sens*, 12 (14) (2020) Art No 2269. https://doi.org/10.3390/rs12142269

25 ICMAM (Integrated Coastal and Marine Area Management), Government of India, *Critical Habitat Information System for Gulf of Khambhat-Gujarat*, Report of Government of India, 2002, pp. 7-11.

26 Pahlevan N, Sarkar S, Franz B A, Balasubramanian S V & He J, Sentinel-2 MultiSpectral Instrument (MSI) data processing for aquatic science applications: Demonstrations and validations, *Remote Sens Environ*, 201 (2017) 47–56. https://doi.org/10.1016/j.rse.2017.08.033

27 Seleem T, Bafi D, Karantzia M & Parcharidis I, Water quality monitoring using Landsat 8 and Sentinel-2 satellite data (2014–2020) in Timsah Lake, Ismailia, Suez Canal Region (Egypt), *J Indian Soc Remote Sens*, 50 (12) (2022) 2411–2428. https://doi.org/10.1007/s12524-022-01613-9

28 Maslukah L, Basayep I, Wirasatriya A, Indrayanti E, Prasetyawan I B, *et al.*, Application of Sentinel-2 imagery for total suspended solids mapping off the Bodri River, Kendal Regency, Indonesia, *Remote Sens Appl Soc Environ*, 36 (2024) p. 101379. https://doi.org/10.1016/j.rsase.2024.101379

29 Pahlevan N, Smith B, Alikas K, Anstee J, Barbosa C, *et al.*, Simultaneous retrieval of selected optical water quality indicators from Landsat-8, Sentinel-2, and Sentinel-3, *Remote Sens Environ*, 270 (2022) p. 112860. https://doi.org/10.1016/j.rse.2021.112860

30 Priyaa S S, Ramesh S & Ramadas G A, Retrieval of water quality parameters of South Andaman coral Islands using remotely operated underwater vehicle, *Water Sci*, 33 (1) (2019) 105–117. https://doi.org/10.1080/11104929.2019.1662649

31 Mueller J L, SeaWiFS algorithm for the diffuse attenuation coefficient, K(490), using water-leaving radiances at 490 and 555 nm, In: *SeaWiFS Postlaunch Calibration and Validation Analyses*, Part 3, edited by S B Hooker, (NASA Goddard Space Flight Centre, Greenbelt, Maryland), 2000, pp. 24–27.

32 Lee Z, Darecki M, Carder K L, Davis C O, Stramski D, *et al.*, Diffuse attenuation coefficient of downwelling irradiance: An evaluation of remote sensing methods, *J Geophys Res*, 110 (C2) (2005) p. C02017. https://doi.org/10.1029/2004JC002573

33 Misra A, Mani M R, Soniya S & Vethamony P, Seasonal variations of total suspended matter (TSM) in the Gulf of Khambhat, west coast of India, *Indian J Geo-Mar Sci*, 43 (7) (2014) 1202-1209. http://nopr.niscpr.res.in/handle/12345-789/34422

34 Arnone R A, Lee Z P, Martinolinch & Ladner S D, Characterizing the optical properties of coastal waters by coupling 1 km and 250 m channels on MODIS- Terra, In: *Proc Ocean Opt XVI*, Sante Fe, NM, 2002, pp. 1-15.

35 Pradhan Y, Rajawat A S & Nayak S, Application of IRS-P4 OCM data to study the impact of tidal propagation on sediment dynamics in the Gulf of Kachch, *Indian J Geo-Mar Sci*, 32 (2) (2004) 129-137. http://nopr.niscpr.res.in/handle/123456789/1658